



Article

Magnetic Field Suppression of the Martensitic Transformation in Mn-Based MnNi(Fe)Sn Metamagnetic Shape Memory Heusler Alloys

Patricia Lázpita ^{1,2,*}, Natalia Ahiova Río-López ^{1,2}, David Mérida ¹, Emily (Leonie Quinlyn Nowalaja) Ammerlaan ³, Uli Zeitler ³, Volodymyr Chernenko ^{1,2} and Jon Gutiérrez ^{1,2,*}

- Department Electricity and Electronics, Faculty of Science and Technology, University of the Basque Country UPV/EHU, Barrio Sarriena s/n, 48940 Leioa, Spain; nataliaahiova.rio@ehu.eus (N.A.R.-L.); david.merida@ehu.eus (D.M.); volodymyr.chernenko@ehu.eus (V.C.)
- ² BCMaterials, Martina Casiano Building, UPV/EHU Scientific Park, Barrio Sarriena s/n, 48940 Leioa, Spain
- ³ High Field Magnet Laboratory (HFML-EMFL), Radboud University, 6525 ED Nijmegen, The Netherlands; nowa.ammerlaan@ru.nl (E.A.); uli.zeitler@ru.nl (U.Z.)
- * Correspondence: patricia.lazpita@ehu.eus (P.L.); jon.gutierrez@ehu.eus (J.G.)

Abstract

Heusler-type metamagnetic shape memory alloys (MMSMAs) exhibit a large functional response associated with a first-order martensitic transformation (MT). The strong magneto-structural coupling combined with the presence of mixed magnetic interactions enables controlling this MT by means of a magnetic field, resulting in different multifunctional properties, among them giant magnetoresistance, metamagnetic shape memory effect (MMSM), or inverse magnetocaloric effect (MCE). Not only the shift rate of MT as a function of the magnetic field but also its eventual suppression are key parameters in order to develop these effects. Here we present our findings concerning a detailed study of the magnetic field-induced MT and its suppression in MnNi(Fe)Sn MMSMAs, by applying strong steady magnetic fields up to 33 T. These measurements will lead to the creation of the T- $\mu_0 H$ phase diagrams of the MT. Moreover, we will also give light to the effect of Fe—content and, as a direct consequence, the magnetic coupling on the suppression of the magnetostructural transformation.

Keywords: heusler metamagnetic shape memory alloy; martensitic transformation; kinetic arrest; magnetic field phase diagram



Received: 7 July 2025 Revised: 24 September 2025 Accepted: 10 October 2025 Published: 16 October 2025

Citation: Lázpita, P.; Río-López, N.A.; Mérida, D.; Ammerlaan, E.; Zeitler, U.; Chernenko, V.; Gutiérrez, J. Magnetic Field Suppression of the Martensitic Transformation in Mn-Based MnNi(Fe)Sn Metamagnetic Shape Memory Heusler Alloys. Magnetism 2025, 5, 25. https:// doi.org/10.3390/magnetism5040025

Copyright: © 2025 by the authors. Licensee MDPI, Basel, Switzerland. This article is an open access article distributed under the terms and conditions of the Creative Commons Attribution (CC BY) license (https://creativecommons.org/licenses/by/4.0/).

1. Introduction

Heusler metamagnetic shape memory alloys (MMSMAs) of the Ni-Mn-X (X = In, Sn, Sb)-type exhibit good physical properties and a remarkable functional response associated with a first-order martensitic transformation (MT) [1,2]. In these compounds, the combination of magneto-volume coupling and diverse ferromagnetic—antiferromagnetic interactions allows for control of this MT by using an external magnetic field through the effect of magnetic field-induced martensitic transformation (MFIMT). This leads to multifunctional properties, such as the magnetocaloric [3,4] magnetoresistance, magnetostrain and metamagnetic shape memory [5,6] effects, paving the way for technical applications.

Magnetism **2025**, 5, 25

When controlled by a magnetic field, this metamagnetic transformation is directly related to the magnetization change between the austenitic and martensitic phases at the MT. The well-known Clausius–Clapeyron relationship:

$$-\frac{dT_M}{d(\mu_0 H)} = \frac{\Delta M}{\Delta S} \tag{1}$$

where μ_0H is the applied magnetic field, T_M is the MT temperature and ΔM and ΔS are the magnetization and entropy changes at the MT, respectively, providing insights into the advantages of searching for alloys that exhibit large ΔM and high magnetostructural coupling, resulting in large $\mathrm{d}T_M/\mathrm{d}\mu_0H$ values, thereby facilitating the magnetic field-induced transformation and maintaining a substantial ΔS . To tailor ΔM and T_M , one can modify the composition of the alloy or properly dope it with other elements.

The magnetization in Heusler-like alloys mainly depends on the magnetic moment of Mn atoms and the distance between these atoms, which determine the observed magnetic exchange interactions [7,8]. Clearly, increasing Mn content is a suitable strategy to enhance the ΔM change value, as reported by Xuang et al. [9]. The Mn-Mn magnetic interactions can also be altered by doping with another magnetic element, such as the 3d Fe or Co atoms. For example, in the case of Mn₅₀Ni₄₀In₁₀ alloys, doping with a 3 at.% Co increases magnetization from $40 \text{ Am}^2\text{kg}^{-1}$ to $89 \text{ Am}^2\text{kg}^{-1}$, as reported by Wu et al. [10]. Lázpita et al. [11] reported an increase in ΔM from 19 $\mathrm{Am^2kg^{-1}}$ (x = 0) to 49 $\mathrm{Am^2kg^{-1}}$ (x = 4) in Mn₄₉Ni_{42-x}Fe_xSn₉ alloys. This doping with additional magnetic atoms also promotes the formation of new secondary phases in the alloy, which can be advantageous for enhancing their mechanical characteristics by reducing, for instance, the inherent fragility of these MMSMAs. Moreover, for certain critical concentrations of these dopants, there are changes in the magnetic coupling that can hinder the entire magnetostructural transformation, preventing its progression [12,13]. In these situations, a fascinating phenomenon occurs in MMSMAs, known as the kinetic arrest of MT, which hinders the magnetostructural transition under a sufficiently strong magnetic field [14–16].

The effect of kinetic arrest is related to the total entropy change across the MT, ΔS_T , which must be negative for the direct MT. The total entropy of the MT is expressed as $\Delta S_T = \Delta S_{lattice} + \Delta S_{magnetic}$, where $\Delta S_{lattice}$ and $\Delta S_{magnetic}$ are the lattice and magnetic entropy, respectively (the electronic entropy contribution can be neglected in these cases). In the MMSMAs, the lattice entropy is negative in the direct MT, while the magnetic entropy is positive and lower, since now the transition occurs from a ferromagnetic to a paramagnetic phase, resulting in $\Delta S_T < 0$. In the presence of a magnetic field, $\Delta S_{lattice}$ remains invariant, while $\Delta S_{magnetic}$ increases, and the lattice contribution to the total entropy remains constant, while the magnetic contribution increases, eventually leading to a zero total entropy $\Delta S_T \sim 0$, inhibiting or kinetically arresting MT at a critical magnetic field.

There are two methods to investigate the kinetic arrest phenomenon through the study of magnetic properties. The first method is to measure the temperature dependence of the magnetization (*M*) at different constant magnetic fields (*H*). The second method is to measure *M* as a function of *H*, at various constant temperatures. Thus, MFIMT and related phenomena can be studied by performing zero field cooling (ZFC) measurements starting from the martensitic phase, or by performing field cooling (FC) measurements starting either from the martensitic or austenitic phases of the alloy [17]. In this last case, the applied field during the FC process can be high enough to arrest the MT. Landazábal et al. [18] argued that this arrest may originate from the fact that "the microstructure obtained after ZFC is stable, but the one obtained after FC is in a non-equilibrium state".

In this study, we report the outcomes of the impact of high magnetic fields on two particular compositions, x = 4 and x = 5, belonging to the previously studied family $Mn_{49}Ni_{42-x}Fe_xSn_9$

Magnetism **2025**, 5, 25 3 of 10

(0 < x < 6) of alloys [11]. In particular, for the alloy with x = 5, we observed both MFIMT and kinetic arrest at approximately 18 T. However, for the alloy with x = 4, we only observed MFIMT, and no kinetic arrest was detected even at magnetic fields up to 33 T. Such behaviors will be explained in terms of lattice and magnetic entropy contributions.

2. Materials and Methods

A detailed description of the fabrication of polycrystalline ingots of $Mn_{49}Ni_{42-x}Fe_xSn_9$ (x = 0, 2, 3, 4, 5 and 6), X-ray structural characterization, as well as the DSC analysis of these samples, has been published in the reference [11].

In particular, and for the alloys with x = 4 and x = 5 Fe content, as the object of discussion of this work, their microstructure was examined by scanning electron microscopy (SEM) in a Hitachi TM300 (Hitachi, Tokyo, Japan) table-top provided with energy-dispersive (EDX) analysis. This EDX allows for establishing composition values with an uncertainty of about 1 at.%.

Thermomagnetic measurements were performed in a vibrating sample magnetometer (VSM) from 10 to 400 K and applied fields H up to 12 T. In order to establish the T- μ_0H phase diagrams for the two studied alloys, we carefully determined the effect of the applied magnetic field on the MT by measuring thermomagnetic curves. The high-temperature part of this diagram was obtained by using a VSM in the range of 5–320 K at constant applied fields up to 12 T (Magnetic platform from Cryogenic Ltd. CFMS, London, UK). Martensitic transformation temperatures for each applied field were determined by the conventional two-tangent method. The low temperature region of each phase diagram was determined through isothermal magnetization curves measured from 250 K down to 4.2 K and under applied fields up to 33 T at the High Field Magnet Laboratory (HFML-EMFL, Radboud University, Nijmegen, The Netherlands). At these low temperatures, it is necessary to have such a strong magnetic field to ensure the largest possible completeness for both the reverse and forward MFIMT.

3. Results and Discussion

3.1. Crystal Structure and Microstructure

Room temperature X-ray diffraction patterns have revealed three different crystal structures in bulk samples as the Fe content in their composition varies [11]. The x = 4 composition alloy shows a mixture of three phases: cubic austenite, orthorhombic martensite and fcc γ -phase. The latter arises from the addition of iron. However, the alloy corresponding to x = 5 exhibits only the B2 cubic phase with some fcc γ -precipitates. It should be noted that the cell parameters for the austenitic B2 phase (a = 6.01 Å and 5.99 Å for x = 4 and 5, respectively) and the γ -phase (a = 3.73 Å and 3.74 Å for x = 4 and 5, respectively) remain almost constant for both Fe-containing alloys. This behavior contrasts with that previously observed in NiMnSn alloys doped with Fe [19], where iron doping produced a clear increase in the cubic cell parameter.

SEM images analysis of alloys x=4 and 5 show different features (see Figure 1), more specifically, they show two different zones: a continuous, light area corresponding to the matrix and a darker area corresponding to random γ -phase precipitates. From EDX analysis, we have also found a fairly good agreement between the measured average compositions and the expected nominal ones. However, the percentage of the fcc γ -phase in these two alloys is higher in the sample with the highest Fe content: a 13.3 vol.% for the x=4 sample, which increases to 19.1% for the x=5 alloy.

Magnetism **2025**, 5, 25 4 of 10

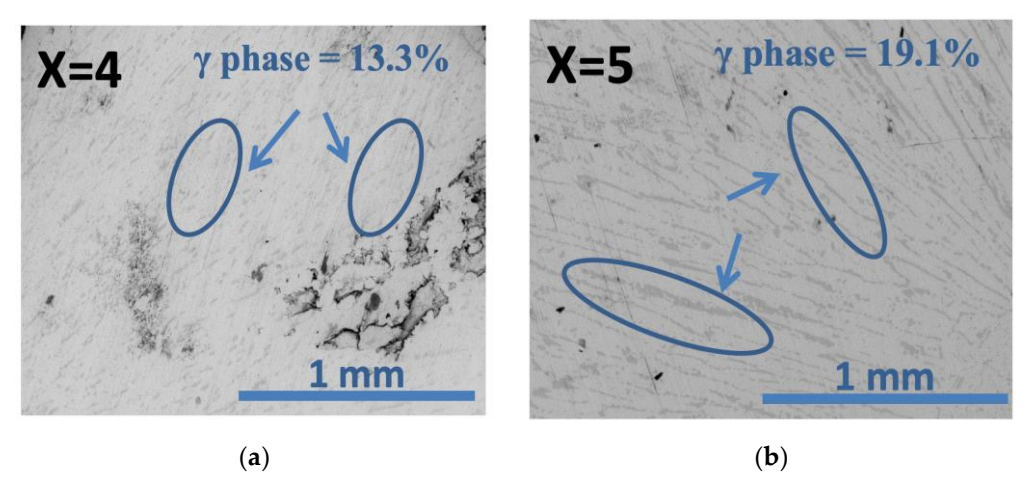


Figure 1. SEM images for $Mn_{49}Ni_{42-x}Fe_xSn_9$ alloys with (a) x = 4 composition (darkest zones correspond to carbon tape-generated contamination) and (b) x = 5 composition.

3.2. Magnetic Field Influence on the Martensitic Transformation and Kinetic Arrest

To magnetically characterize the MT exhibited by these alloys, thermo-magnetization measurements, M(T), at a low magnetic field of 5 mT were performed. These curves are convenient to adequately determine MT temperatures during cooling $T_M = (M_s + M_f)/2$ (where M_s and M_f are the forward MT temperatures, start and finish, respectively), and heating $T_A = (A_s + A_f)/2$ (where A_s and A_f are the reverse MT temperatures, start and finish, respectively) processes, as well as the magnetization change ΔM between the start and the end of the MT, $\Delta M = M^A - M^M$, were M^A and M^M denote magnetization values of the austenite and martensite phases, respectively. Thus, the measured forward MT temperature is about 223 K for the x = 4 sample and decreases for the x = 5 Fe content composition to a transformation temperature of about 80 K. With regard to the magnetization change (ΔM), it was evaluated through thermomagnetic measurements at a magnetic field of 9 T in order to analyze the maximum magnetization difference between the martensite and austenite phases. The measured ΔM value is about 50 Am²kg⁻¹ for the x = 4 alloy and exhibits a sharp drop to $8 \text{ Am}^2 \text{kg}^{-1}$ for the x = 5 composition. Figures 4 and 5 in Reference [11] properly describe this previous MT magnetic characterization for the whole family of Mn₄₉Ni_{42-x}Fe_xSn₉ alloys.

The significant difference observed between the x = 4 and x = 5 composition alloys in terms of thermo-magnetic measurements fully justifies the need for a more in-depth study of their magnetization transformation behavior, in particular, an extensive analysis of the effect of the magnetic field on the MT under different routes as ZFC and FC conditions.

Figure 2 shows recorded thermo-magnetic curves for the x = 4 (measured up to 12 T) and x = 5 (measured up to 9 T). The lowest applied magnetic-field-intensity-measured curve allows for the determination of the Curie temperature of the alloy as the minimum of the dM/dT dependence. Thus, austenite Curie temperatures about 296 K for the x = 4 alloy and 283 K for the x = 5 alloy were determined.

It is evident that the applied magnetic field has a significant influence on both the MT temperature and the observed ΔM value: by increasing the applied magnetic field, the MT temperatures decrease away from the Curie temperature. This behavior promotes the enhancement of magnetization in both the austenite and martensite phases. However, the evolution of ΔM differs notably between the two alloys. In the x=4 alloy, the magnetic field favors the MT, with ΔM values increasing from 35 to 50 $\Delta m^2 kg^{-1}$ as the applied magnetic field increases from 0 to 12 T. That is, the field-induced magnetization increment in the austenite phase is greater than that in the martensite phase. In contrast, the x=5 alloy exhibits a decrease in ΔM from 20 to 10 $\Delta m^2 kg^{-1}$ as the magnetic field increases from

Magnetism **2025**, 5, 25 5 of 10

0 to 9 T. This alloy experiences a significant ΔM increase at low applied fields (up to 0.7 T), followed by a decrease at higher magnetic fields, indicating that the magnetic field H can inhibit the MT.

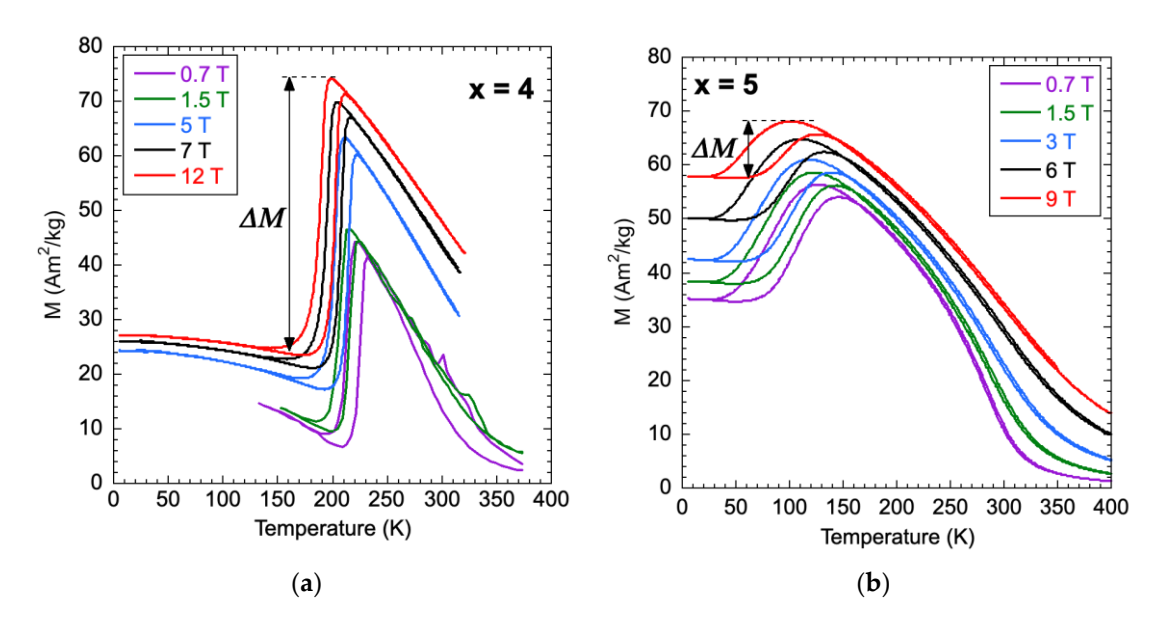


Figure 2. Thermo-magnetization curves measured for $Mn_{49}Ni_{42-x}Fe_xSn_9$ alloys with (**a**) x = 4 composition and (**b**) x = 5 composition.

To further analyze this observed behavior, we measured isothermal magnetization curves M(H) under ZFC conditions above and below the corresponding MT temperatures for both alloys. Figure 3a shows such measurements for the x = 4 Fe content alloy ($T_M = 223$ K). The curve recorded at 230 K is clearly in the ferromagnetic austenite phase. Curves measured at 200 and 174 K, temperatures where only the martensite structure is expected to appear within this alloy, show an increase in the magnetization value when the magnetic field is applied, indicating MFIMT, which starts at the austenitic start magnetic field (H_{AS}) with a reversible metamagnetic effect. The measured behavior goes from the low magnetization value of the weak-magnetic martensite to the high magnetization one of the ferromagnetic austenite. The measurement performed at 151 K shows the remaining martensite magnetization, as expected, and is much lower than the austenite one. At this temperature, a full MFIMT is not observed for magnetic fields up to 33 T, displaying only a small increment in the magnetization trend related to a partial MT. Figure 3b shows graphically measured magnetization values determined in FC conditions where the MT takes place completely under 30 T of the applied magnetic field, i.e., there is no arrested austenite, and the kinetic arrest effect does not occur. The inset clearly indicates that at a low temperature (142 K in Figure 3b), the alloy presents a weakly magnetic martensite, which is not affected by the cooling conditions, showing the same behavior for ZFC and FC protocols.

The measured isothermal magnetization curves M(H) together with the isomagnetic field magnetization ones M(T) also allow for the construction of a T- μ_0H phase diagram of the characteristic temperatures of the MT. This is shown in Figure 4.

As observed, there is a quasi-linear dependence of all determined $A_{s,f}$ and $M_{s,f}$ temperature values, with a negative slope of about -2.25 K/T, practically equal for all of these transformation temperatures. In addition, kinetic arrest of the MT has not been reached for applied magnetic fields as high as ~30 T. The lack of data for $M_{f,s}$ at high applied magnetic fields is just due to experimental setup limitations.

Magnetism **2025**, 5, 25 6 of 10

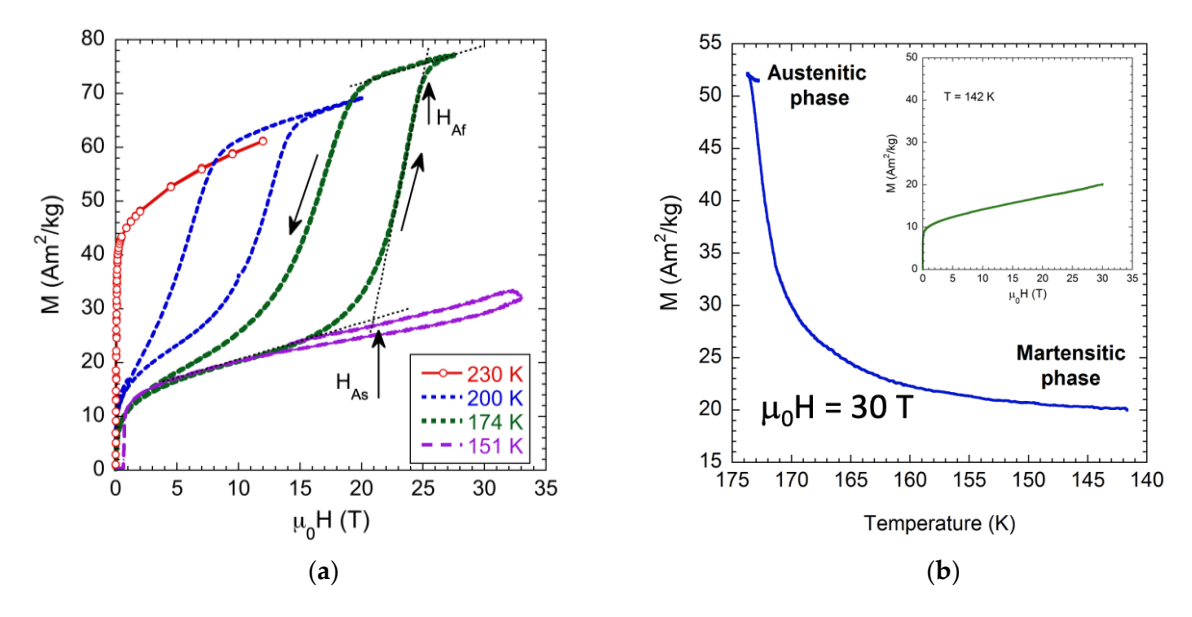


Figure 3. (a) ZFC magnetization loops (at the first quadrant) at different temperatures and a maximum applied H field of 33 T measured for the x = 4 Fe content alloy. (b) Measured magnetization evolution as a function of temperature at an applied H field of 30 T. The inset shows the magnetic field-induced magnetization of the martensite, measured at 142 K after a 30 T FC condition.

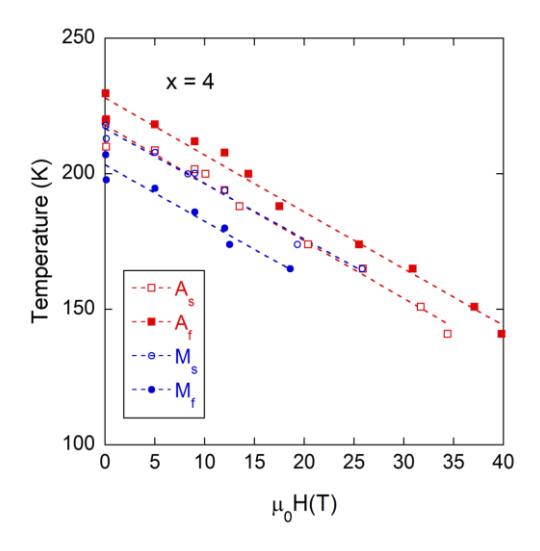
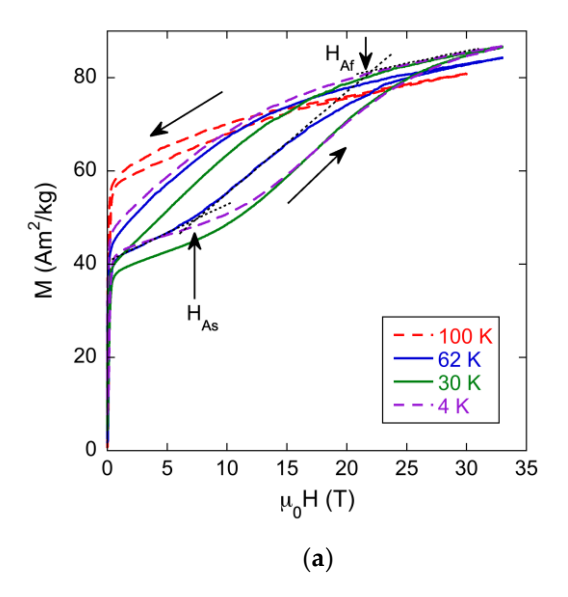


Figure 4. T- $\mu_0 H$ phase diagram of the characteristic temperatures of the MT for the Mn₄₉Ni₃₈Fe₄Sn₉ alloy (x = 4). Note that the error bars fall within the size of the data points.

Figure 5a shows similar measurements performed for the x=5 Fe content alloy ($T_M=80$ K). The curve recorded at 100 K is in the austenite phase and shows mostly a ferromagnetic behavior. The loops measured at 62 K (practically at the end of the MT) and 30 K (at the martensite phase) are quite similar in shape, and clearly, the martensitic phase contribution to magnetization at low magnetic field and a partial reversible MFIMT, which starts at $H_{AS}=7$ T and 11 T, is observed. Finally, the curve measured at 4 K presents a similar behavior, but its width increases, indicating that the reversibility of the MFIMT is restricted and that the fraction of the non-transformed martensite increases due to the magnetic field austenite phase arrest. Moreover, the austenitic phase obtained across the MFIMT is stable over a larger field range as the temperature decreases. Also, the measured magnetization value at the highest applied field of 33 T, at those previous temperatures, slightly increases, indicating that a higher percentage of austenite phase is induced, although it can also be explained by increased saturation magnetization at low temperatures. Figure 5b shows

Magnetism **2025**, 5, 25 7 of 10

the measured M(H) behavior at 4 K when this temperature is reached in ZFC and FC conditions. While the shape of the two loops is quite similar, it turns out to be lower than the martensitic saturation magnetization when it is measured after ZFC conditions. This fact clearly indicates that the FC protocol partially retains the MT, with the presence of a ferromagnetic austenite phase that reflects in the increase in the saturation magnetization at low magnetic field. Moreover, at this low temperature, the applied magnetic field is still able to induce some transformation of the martensite. The H_{AS} is higher for the FC protocol due to the lower fraction of martensitic phase that can transform in this case.



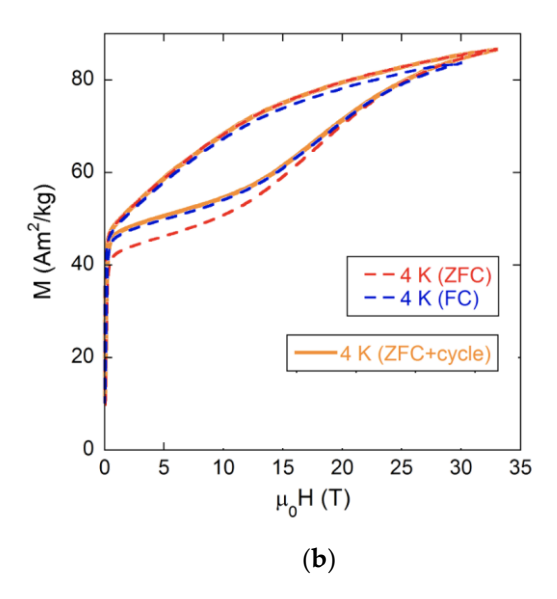


Figure 5. (a) Magnetization loops (in the first quadrant) measured at different temperatures for the x = 5 Fe content alloy. (b) Magnetization loops (in the first quadrant) at 4 K and measured under ZFC and FC conditions. In both cases, a maximum applied H field of 33 T has been used.

Again, from measured isothermal magnetization curves M(H), the $T-\mu_0H$ phase diagram of the characteristic temperatures of the MT can be constructed. This is shown in Figure 6. The behavior of MT temperatures is now drastically different from that previously shown for the x = 4 alloy. At temperatures above 50 K, transformation characteristic temperatures decrease in a strong non-linear manner as the applied magnetic field increases. Nevertheless, at temperatures lower than 50 K, two behaviors can be observed: on the one hand, applied magnetic fields required to induce the reverse MT are practically constant, up to 4 K, and do not change with decreasing temperature (H_{As} about 11 T and H_{Af} about 25 T). On the other hand, applied magnetic fields required to induce the direct MT are lower when temperatures drop, reaching a minimum of 14 T at 4 K. In fact, at the lowest temperatures, there is a remarkable split between the M_s and A_f temperature evolution curves. This observation arises from the fact that ZFC or FC processes below 50 K have a different impact on the state (either stable or non-equilibrium, depending on the cooling process) of the martensite phase of the x = 5 sample. The lack of data for M_f at the lowest temperatures is related to the fact that the direct MT is partially inhibited when it occurs after the application of a magnetic field. Then, Figure 5 represents what is already known in MMSMAs as the kinetic arrest effect [14-16] in which the austenite phase is, for this x = 5 alloy, "frozen" or "blocked" for applied magnetic fields higher than ~17 T.

Based on our observations, we can explain the distinct behavior of our $Mn_{49}Ni_{42-x}Fe_xSn_9$ alloys with x=4 and x=5 by considering the influence of the Fe content on the magnetic and martensitic transition (MT) characteristics of these two compositions. Neither of these alloys exhibits magnetic saturation for applied magnetic fields up to 33 T, which clearly indicates the

Magnetism **2025**, 5, 25 8 of 10

presence of antiferromagnetic (AFM) coupling when Ni atoms are substituted by Fe. A slight change in the Fe content, from x = 4 to x = 5, leads to a drastic alteration in the magnetization change, ΔM , of each alloy. Evaluating the ZFC isothermal magnetization curves, the x = 4 alloy exhibits a maximum ΔM value of about 50 Am²kg⁻¹ at 174 K, while the x = 5 alloy shows just a maximum ΔM value of 30 Am²kg⁻¹ at 30 K; moreover, both values remain almost constant when the martensitic transformation is fully developed. This variation represents a 40% reduction in the magnetization change when the Fe doping increases by 1%. If we assume that the austenitic phase saturation magnetization is similar in both alloys (around 80 Am²kg⁻¹), the ΔM decrease can be related to the increase in the magnetization of the martensitic phase, indicating that the Fe doping favors the ferromagnetic coupling over the antiferromagnetic one of the martensitic phase. This change in magnetic coupling would directly impact the magnetic entropy variation in the transformation $\Delta S_{magnetic}$, allowing the arrested kinetic process for the higher Fe alloy.

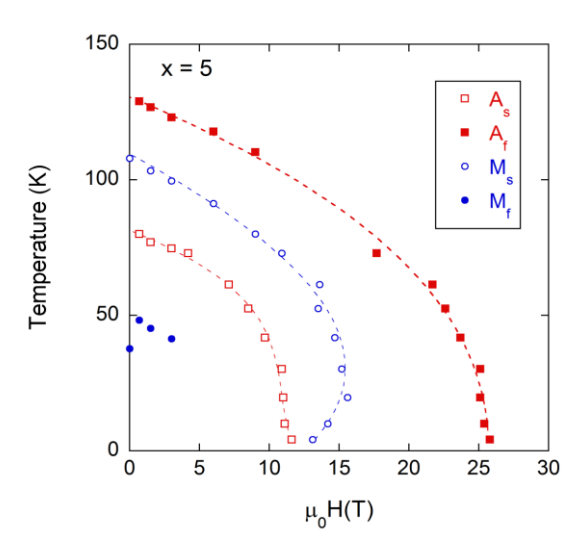


Figure 6. Transformation temperatures versus magnetic field diagram for the $Mn_{49}Ni_{37}Fe_5Sn_9$ alloy. Note that the error bars fall within the size of the data points.

Analyzing the observed behavior in terms of entropy change, which is considered to arise from lattice vibrational and magnetic contributions, $\Delta S = \Delta S_{lattice} - \Delta S_{magnetic}$, and assuming that $\Delta S_{lattice}$ is not influenced by the applied magnetic field, it is clear that the cooling process of the alloys during measurements, as well as the presence of retained austenite at very low temperatures, directly influence the $\Delta S_{magnetic}$ magnitude. In the case of $|\Delta S_{lattice}| = |\Delta S_{magnetic}|$, $\Delta S \sim 0$, and the kinetic arrest occurs. This is the situation shown in Figure 6 for the x = 5 alloy. Most probably, this kinetic arrest is also enhanced by the present amount of γ -phase inside this alloy: as previously stated, while for the x = 4 alloy composition, a vol.% of 13.3 has been determined, and this percentage increases up to 19.1 for the x = 5 alloy. Precipitates increase the internal stresses, which could favor the appearance of the kinetic arrest in the latter alloy.

4. Conclusions

The Fe doping of Mn-Ni-Sn metamagnetic alloys opens up the possibility to study a wide range of magnetic field-induced phenomena, such as changes in magnetization (ΔM), changes in the MT temperatures (T_M) and the associated transformation entropy (ΔS), and even the occurrence of the kinetic arrest process. Slight changes in the composition of Mn₄₉Ni_{42-x}Fe_xSn₉ alloys from x = 4 to 5 result in completely different behaviors. The alloy with x = 4 shows large ΔM = 50 Am²kg⁻¹ at 174 K and MT temperatures A_{sf} and M_{sf} with a negative slope of about -2.25 K/T for applied magnetic fields up to 40 T, and there is no trace of kinetic arrest

Magnetism 2025, 5, 25 9 of 10

of MT at these high applied fields. In contrast, the x = 5 alloy exhibits a significantly reduced $\Delta M = 30~{\rm Am^2kg^{-1}}$ at 30 K. The MT temperatures evolve in a strongly non-linear manner as the temperature decreases and the applied magnetic field increases. For applied magnetic fields greater than ~17 T, the MT kinetic arrest occurs. The origin of this kinetic arrest can be attributed to the amount of retained austenite in the Mn₄₉Ni₃₇Fe₅Sn₉ alloy. This is likely favored not only by the cooling process under a magnetic field during the measurements, but also by the presence of the fcc γ -phase in the alloy.

Author Contributions: Conceptualization, P.L., V.C. and J.G.; methodology, P.L., N.A.R.-L., D.M. and V.C.; validation, N.A.R.-L., D.M., E.A. and U.Z.; investigation, N.A.R.-L., D.M., E.A. and U.Z.; writing—original draft preparation, P.L. and J.G.; supervision, J.G.; project administration, J.G. and P.L. All authors discussed the results and contributed to the final manuscript. All authors have read and agreed to the published version of the manuscript.

Funding: This research was funded by the Grant PID2022-138108OB-C33 funded by MICIU/AEI/ 10.13039/501100011033, Project IT1479-22 and Project IKUR_IKA_25/03.

Institutional Review Board Statement: Not applicable.

Informed Consent Statement: Not applicable.

Data Availability Statement: The data are contained within the article.

Acknowledgments: P.L., N.A.R.-L., D.M. and J.G. gratefully acknowledge the Spanish Ministerio de Ciencia, Innovación y Universidades, for financial support under Grant PID2022-138108OB-C33 funded by MICIU/AEI/10.13039/501100011033 and by the European Union Next Generation EU/PRTR. The financial support of the Basque Government under the Research Groups Program IT1479-22 project and research project IKUR_IKA_25/03 (Ikerbasque Foundation, Basque Foundation for Science, Basque Government) is also acknowledged. Technical and human support provided by the General Research Services of the UPV/EHU (SGIker) is gratefully acknowledged.

Conflicts of Interest: The authors declare no conflicts of interest.

Abbreviations

The following abbreviations are used in this manuscript:

MMSMA Heusler metamagnetic shape memory alloy

MT Martensitic transformation

MMSM Metamagnetic shape memory effect

MCE Magnetocaloric effect

MFIMT Magnetic field-induced transformation

FC Field cooling
ZFC Zero field cooling

DSC Differential scanning calorimetry
SEM Scanning electron microscopy
EDX Energy-dispersive X-ray analysis

VSM Vibrating sample magnetometry/magnetometer

AFM Antiferromagnetic

References

- 1. Kainuma, R.; Imano, Y.; Ito, W.; Sutou, Y.; Morito, H.; Okamoto, S.; Kitakami, O.; Oikawa, K.; Fujita, A.; Kanomata, T.; et al. Magnetic-field-induced shape recovery by reverse phase transformation. *Nature* **2006**, 439, 957–960. [CrossRef] [PubMed]
- 2. Yu, S.Y.; Cao, Z.X.; Ma, L.; Liu, G.D.; Chen, J.L.; Wu, G.H.; Zhang, B.; Zhang, X.X. Realization of magnetic field-induced reversible martensitic transformation in NiCoMnGa alloys. *Appl. Phys. Lett.* **2007**, *91*, 102507. [CrossRef]
- 3. Krenke, T.; Duman, E.; Acet, M.; Wassermann, E.F.; Moya, X.; Mañosa, L.; Planes, A. Inverse magnetocaloric effect in ferromagnetic Ni-Mn-Sn alloys. *Nat. Mater.* **2005**, *4*, 450–454. [CrossRef] [PubMed]

Magnetism **2025**, 5, 25

4. Castillo-Villa, P.O.; Mañosa, L.; Planes, A.; Soto-Parra, D.E.; Sánchez-Llamazares, J.L.; Flores-Zúñiga, H.; Frontera, C. Elastocaloric and magnetocaloric effects in Ni-Mn-Sn(Cu) shape-memory alloy. *J. Appl. Phys.* **2013**, *113*, 053506. [CrossRef]

- 5. Kainuma, R.; Oikawa, K.; Ito, W.; Sutou, Y.; Kanomata, T.; Ishida, K. Metamagnetic shape memory effect in NiMn-based Heusler-type alloys. *J. Mater. Chem.* **2008**, *18*, 1837. [CrossRef]
- 6. Ito, K.; Ito, W.; Umetsu, R.Y.; Tajima, S.; Kawaura, H.; Kainuma, R.; Ishida, K. Metamagnetic shape memory effect in polycrystalline NiCoMnSn alloy fabricated by spark plasma sintering. *Scr. Mater.* **2009**, *61*, 504–507. [CrossRef]
- 7. Enkovaara, J.; Heczko, O.; Ayuela, A.; Nieminen, R.M. Coexistence of ferromagnetic and antiferromagnetic order in Mn-doped Ni₂MnGa. *Phys. Rev. B* **2003**, *63*, 212405. [CrossRef]
- 8. Richard, M.L.; Feuchtwanger, J.; Allen, S.M.; O'Handley, R.C.; Lazpita, P.; Barandiarán, J.M.; Gutiérrez, J.; Ouladdiaf, B.; Mondelli, C.; Lograsso, T.A.; et al. Chemical order in off-stoichiometric Ni-Mn-Ga ferromagnetic shape-memory alloys studied with neutron diffraction. *Philos. Mag. A* 2007, 87, 3437–3447. [CrossRef]
- 9. Xuang, H.C.; Ma, S.C.; Cao, Q.Q.; Wang, D.H.; Du, Y.W. Martensitic transformation and magnetic properties in high-Mn content Mn₅₀Ni_{50-x}In_x ferromagnetic shape memory alloys. *J. Alloy Comp.* **2011**, *509*, *5761*–*5764*. [CrossRef]
- 10. Wu, Z.; Liu, Z.; Yang, H.; Liu, Y.; Wu, G. Metamagnetic phase transformation in Mn₅₀Ni₃₇In₁₀Co₃ polycrystalline alloy. *Appl. Phys. Lett.* **2011**, *98*, 61904. [CrossRef]
- 11. Lázpita, P.; Sasmaz, M.; Barandiarán, J.M.; Chernenko, V.A. Effect of Fe doping and magnetic field on martensitic transformation of Mn-Ni(Fe)-Sn metamagnetic shape memory alloys. *Acta Mater.* **2018**, *155*, 95–103. [CrossRef]
- 12. Wu, Z.; Liu, Z.; Yang, H.; Liu, Y.; Wu, G.; Woodward, R.C. Metallurgical origin of the effect of Fe doping on the martensitic and magnetic transformation behaviours of Ni₅₀Mn_{40-x}Sn₁₀Fe_x magnetic shape memory alloys. *Intermetallics* **2011**, *19*, 445–452. [CrossRef]
- 13. Tan, C.; Tai, Z.; Zhang, K.; Tian, X.; Cai, W. Simultaneous enhancement of magnetic and mechanical properties in Ni-Mn-Sn alloy by Fe doping. *Sci. Rep.* **2017**, *7*, 43387. [CrossRef] [PubMed]
- 14. Ito, W.; Ito, K.; Umetsu, R.Y.; Kainuma, R.; Koyama, K.; Watanabe, K.; Fujita, A.; Oikawa, K.; Ishida, K.; Kanomata, T. Kinetic arrest of martensitic transformation in the NiCoMnIn metamagnetic shape memory alloy. *Appl. Phys. Lett.* **2008**, 92, 021908. [CrossRef]
- 15. Xu, X.; Ito, W.; Tokunaga, M.; Umetsu, R.Y.; Kainuma, R.; Ishida, K. Kinetic arrest of martensitic transformation in NiCoMnAl metamagnetic shape memory alloy. *Mater. Trans.* **2010**, *51*, 1357–1360. [CrossRef]
- 16. Umetsu, R.Y.; Xu, X.; Ito, W.; Kihara, T.; Takahashi, K.; Tokunaga, M.; Kainuma, R. Magnetic field-induced reverse martensitic transformation and thermal transformation arrest phenomenon of Ni₄₁Co₉Mn₃₉Sb₁₁ alloy. *Metals* **2014**, *4*, 609–622. [CrossRef]
- Lázpita, P.; Pérez-Checa, A.; Barandiarán, J.M.; Ammerlan, A.; Zeitler, U.; Chernenko, V.A. Suppression of martensitic transformation in Ni-Mn-In metamagnetic shape memory alloy under very strong magnetic field. *J. Alloys Compd.* 2021, 874, 159814. [CrossRef]
- 18. Pérez-Landazábal, J.I.; Recarte, V.; Sánchez-Alarcos, V.; Gómez-Polo, C.; Kustov, S.; Cesari, E. Magnetic field induced martensitic transformation linked to the arrested austenite in a Ni-Mn-In-Co shape memory alloy. *J. Appl. Phys.* **2011**, *109*, 093515. [CrossRef]
- Aguilar-Ortiz, C.O.; Soto-Parra, D.E.; Alvarez-Alonso, P.; Lázpita, P.; Salazar, D.; Castillo-Villa, P.O.; Flores-Zúñiga, H.; Chernenko, V.A. Influence of Fe doping and magnetic field on martensitic transition in Ni-Mn-Sn melt-spun ribbons. *Acta Mater.* 2016, 107, 9–16. [CrossRef]

Disclaimer/Publisher's Note: The statements, opinions and data contained in all publications are solely those of the individual author(s) and contributor(s) and not of MDPI and/or the editor(s). MDPI and/or the editor(s) disclaim responsibility for any injury to people or property resulting from any ideas, methods, instructions or products referred to in the content.